A numerical study of wall pressure and granular flow in a flat-bottomed silo

A numerical study of wall pressure and granular flow in a flat-bottomed silo

Yin Wang[1,2,*], Yong Lu[3], Jin Y. Ooi[3]

[1] Institute of Geotechnical Engineering, School of Civil Engineering, Dalian University of Technology, Dalian, 116024, China

[2] State Key Laboratory of Coastal and Offshore Engineering, Dalian University of Technology, Dalian, 116024, China

[3]Institute for Infrastructure and Environment, School of Engineering, The University of Edinburgh, Edinburgh, EH9 3JL, UK

Abstract

This paper presents a numerical study of the granular flow in the discharge of a flat-bottomed model silo. The behaviour of the stored granular material is modelled using the finite element (FE) method based on an Arbitrary Lagrangian-Eulerian (ALE) frame of reference, which has shown advantageous performance over the classical FE methods in simulating the silo filling and discharge process in a series of studies leading up to this investigation. Experimental results have been used to validate the computational model using the ALE technique. The spatial distribution and time history of the pressures acting on the vertical silo walls predicted by the FE model are found to resemble well the test results. A semi-mass flow pattern has been predicted by the numerical model, which is very consistent with the corresponding experimental observation. With the validated numerical model, the flow behaviour specifically under a flat-bottomed geometry of silos is examined. Based on the velocity distribution in the granular material, a critical velocity ratio criterion is proposed and used to

identify the flow channel boundary. A further numerical study has shown that the flow behaviour in the flat-bottomed silo is closely related to the shear strength of the material, which is represented by the internal friction angle for the cohesionless sand considered in the present study.

Keywords: finite element modelling; Arbitrary Lagrangian-Eulerian formulation (ALE); wall pressure; granular flow

*Corresponding author. Tel.: +86 411 84708511-810; E-mail address: y.wang@dlut.edu.cn

1. Introduction

Silos and hoppers are commonly applied in the storage, handling and transportation of bulk solids in industries. Since the end of the 19th century [1], silo behaviour in terms of pressure and flow has been extensively studied and progressive advances in knowledge have been achieved [2-7]. However, many aspects concerning the silo structure design still remain unresolved [8]. The determination of the pressures acting on the silo walls, which constitute the main loads in silo design, is an important one. Earlier studies of silo pressure suggest that the wall pressures during filling and storage can be well represented by Janssen type pressure equations [5,9,10]. However, there has been no consensus with regard to the discharge pressure due to its complex time and spatial variations. With a general lack of understanding and information on the discharge process, most national standards have defined silo discharge pressure using simply a multiplier applied to the filling pressure based on Janssen's theory and its modified versions [11]. As a matter of fact, the prediction of the wall pressures during discharge is particularly challenging, as the pressure tends to exhibit significant fluctuations and its distributions

along the silo walls depend closely on the flow pattern developed throughout the silo. More work is still required to understand the detailed development of the flow pattern and the dynamic phenomenon so that the discharge pressure can be determined more accurately.

Concerning the general flow behaviour during discharge of silos, numerous experimental studies have been carried out [6, 12-16]. General characterisation of the funnel flow, which may be subdivided into the semi-mass flow and the internal funnel flow, has been established for the flat-bottomed silos. In both types of funnel flow, some particles are stationary and there is a flow channel boundary separating the flowing and static particles. The difference between the two flows is that in the internal funnel flow the flowing particles do not come into contact with the silo walls, while in the semi-mass flow the flow boundary intersects the silo wall at some level.

The advancement in numerical methods and computer technology have also led increasing use of numerical simulation to study flow behaviour in silos [17-23]. Whilst the finite element method is commonly adopted in analyzing the flow in silos, one of the difficulties is the handling of mesh distortion due to the large deformation of the stored solid during discharge. In many previous studies, either a remesh-rezoning technique or an assumed failure boundary had to be used to describe the flow pattern developed in a silo during discharge in order to resolve the mesh distortion problem [24, 25]. A new technique, known as the arbitrary Lagrangian-Eulerian (ALE) formulation, has been developed to combine the desired features of both the Lagrangian and the Eulerian approaches, particularly in describing the behaviour of solids under large deformations [26]. This technique has been applied to model the granular flow, and so far some satisfactory results have been obtained concerning the silo processes [21, 27-29].

This paper presents a finite element (FE) simulation of pressure and flow in a flat-bottomed silo using an uncoupled Arbitrary Lagrangian-Eulerian (ALE) technique in the Abaqus/Explicit code [27] as part of a series of studies on the dynamic silo behaviour during discharge [28, 29]. The ALE approach allows for the simulation of almost the entire silo discharge process without causing the mesh distortion problem. The geometry of the FE model is made the same as a silo experimentally studied at the University of Edinburgh [30] which is the derivative one of the original Danish silo [5], so that comparisons can be made directly. For completeness of the presentation, the key experimental results which are used in the present study are recapped and discussed in some necessary detail. The FE model is validated by comparing with the experimental results in terms of wall pressure and flow pattern in the silo. Through examining the velocity field in the silo, the Flow Channel Boundary (FCB) can be identified using a proposed FCB criterion for flat bottomed silos. A parametric study with respect to the effect of the internal friction angle of the granular material on flow behaviour in a flat bottomed silo has been performed. As far as the numerical study in this paper is concerned, the focus has been placed on the macroscopic phenomenon of discharge and the development of dynamic pressure on silo walls. For this purpose, a macroscopic elasto-plastic constitutive model (linear Drucker-Prager failure criterion with perfectly plastic flow rule) has been employed. A similar approach has been adopted in various numerical studies in this field [e.g. 24, 25]. The model does not get into detailed shear localization, but it is capable of capturing in a macroscopic perspective the development of shear zones and the associated effect on the dynamic pressure on silo walls, which are deemed to be appropriate for capturing the macroscopic dynamic pressure and flow phenomena.

2. Overview of the experiment

The silo experiment was carried out in a flat-bottomed silo at the University of Edinburgh in the

author's pervious study[30]. Dry sand without cohesion was used as the stored material in the silo. The silo consisted of a cylindrical part with a flat bottom, as shown in Fig.1. The cylindrical part, which was made of epoxy walls of thickness 0.02 m, had an aspect ratio of about 6 (height 4.0 m, diameter 0.7 m). The outlet at the centre of the bottom is circular with a diameter of 0.04m (see Fig.2). In the silo walls were installed a total of 56 normal pressure measuring cells at eight levels: seven cells were allocated at each level and spaced 45^{o} apart around the circumference (see Fig.2). The pressure cells were mounted flushed on the inside of the silo walls and were covered with an epoxy adhesive mixed with sand. In this way the cells did not introduce any imperfections on the silo walls, or cause any change in wall friction [5]. Seven pressure cells, distributed along the same vertical line (labelled 5 at Generatrix 225^{o}, see Fig.2) are selected in the present study, and the normal pressure distribution along this vertical line are obtained from the recorded data. The seven selected cells, namely A5, B5, C5, D5, F5, G5 and H5,were located at the level of 0.35m, 0.7 m, 1.05 m, 1.4 m, 2.1 m, 2.8 m and 3.5 m, respectively, above the silo bottom. Cell E5 was reported to be not working properly and thus was not considered in the present study.

Fig.1 The experimental setup

Fig.2 Schematic diagram of layout of pressure cell on the silo walls

The pressure cells were calibrated before they were mounted in the silo walls [30]. The pressure measurements were controlled using a data acquisition program, which recorded and analysed the data in real time. The recording was performed at 1000 readings per second. The model silo was originally constructed and instrumented by the well known team of Munch-Andersen, Askegaard and Nielsen as part of a very extensive study of silo pressure and flow and the model silo was re-established at the

University of Edinburgh. For details of the full set of measurements and the general measurement reliability, a more detailed description can be found in the reference [5, 31].

Each silo test was conducted as follows. First was the filling process, which took approximately 30 min. A storage period of 26 min followed. Then was the discharge, which took about 40 min. The testing silo facility was designed for distributed filling, which was achieved by feeding the dry sand in such a way that the surface was kept approximately horizontal throughout the filling process. The concentric discharge was operated by opening the outlet at the bottom and the sand was withdrawn under gravity. In this way, a discharge rate of about 0.1 m height fall per minute was recorded.

Fig.3 shows the time histories of normal wall pressures recorded by the seven pressure cells at different height levels. The pressure increased progressively until the end of the filling and then kept almost constant during the storage period. Once discharge started, significant overpressures were recorded by the pressure cells C5, D5, F5 and G5. The instantaneous overpressure seven rose up to about 1 kPa, which was about 25% higher than filing pressure, as recorded by cells D5 and F5 at 1.4 m and 2.1 m above the silo bottom, respectively. In general, the discharge pressure exhibited a characteristic profile of dynamic fluctuations. These fluctuations appeared to show a height-related variation in the amplitude. Above 1.0 m, as recorded by the cells C5, D5, F5, G5 and H5, the wall pressure exhibited strong fluctuations in most of the time during discharge; whereas below 1.0 m, the pressures recorded by the cell A5 and B5 had no significant fluctuations. About the mechanism of the pressure fluctuations in silos, a deeper investigation is given in the authors' previous work [28]. Fig. 4 shows the averaged stress distributions on the silo walls at the end of filling and during discharge. The coefficient of wall friction was averaged by the ratios of the shear stress to the normal wall pressure at different levels and found to be 0.6 for filling and 0.5 for discharge respectively.

Fig.3 Time history of wall normal pressure measured by seven pressure cells at different levels (redrawn after Rotter et al. [30])

Fig. 4 Stress distributions measured to determine the coefficient of wall friction at different levels during filling and discharge in the silo tests (Redrawn after Rotter et al. [30])

The flow pattern during the silo discharge was also examined and the result is schematically demonstrated in Fig.5. The flow pattern was deduced by making direct observation of the intersections of flow boundary on the walls through the semi-transparent silo walls. The semi-mass flow was identified during silo discharge. An effective intersection at the height position of 0.7~1.0 m was recorded and it remained unchanged after about 4 minutes from the start of the discharge. The flow pattern identification was based on multiple observations during the discharge of the dry sand. More sophisticated methods could be used (e.g. [15, 32]), but the result from the direct observation is sufficient to allow a comparison of the flow pattern with the numerical simulation.

Fig.5 Flow channel boundary during the flat-bottomed silo discharge (Redrawn after Rotter et al. [30])

3. Finite element modelling and model validation

3.1 FE model setup and model parameters

The geometry and dimensions of the silo used in the finite element analysis were kept the same as the flat-bottomed silo used in the experiment. In the FE model, the silo was modelled as an axisymmetric problem. A circular outlet was set at the bottom of the silo with a radius of 0.02 m as in the test silo. To avoid mesh distortion, the ALE technique was employed to simulate the mechanical behaviour of the

granular material in the silo during filling, storage and discharge. In using the ALE approach, both Lagrangian and Eulerian boundaries were employed, such that the upper and side surfaces of the stored material in the silo were set to be Lagrangian boundaries while the base (outlet) was considered as an Eulerian boundary, as shown in Fig.6. An adaptive meshing technique was employed to help control the mesh distortion and maintain a high-quality mesh throughout the entire analysis even though large deformation occurred. A fuller description of the ALE boundary definition has been given in previous studies [28, 29].

In the FE simulation, the sand was described using an elastic-perfectly plastic stress-strain relationship with a linear Drucker-Prager failure criterion [33]. The interaction between the walls and sand was modelled using Coulomb type contact with a constant coefficient of wall friction. The sand stored inside the silo was discretised into first-order four-node quadrilateral elements with reduced integration. To ensure satisfactory convergence in the stress results, a fine mesh of 14,000 elements (yielding an element size of 1 cm $\times$ 1 cm) in the present study was employed. The silo walls were considered as an undeformable body and modelled using 200 two-node rigid elements, as shown in Fig.6.

Fig.6 FE mesh configuration and ALE boundaries

Table 1 summarises the material properties for the dry sand used in the FE simulation. The properties were obtained mainly from the silo experiments, except that the Young's modulus and Poisson's ratio, which were not available from the experiments and were chosen in consultation with the relevant literature [6, 34, 35, 36]. An average wall friction coefficient, which is the ratio of the measured shear stress to wall normal pressure as shown in Fig. 4, was determined at different levels at the end of filling

and during discharge in the silo test and was used in the silo filling and discharge simulation respectively. The internal friction angle of the material ϕ_i was approximated by the repose angle of the sand measured in the experiments. This determination of the model parameter from the internal friction angle, ϕ_{DP}, for the Drucker-Prager failure criterion gave an upper and a lower bound value respectively using the correction equation in Abaqus [27] as below:

$$\frac{3\sin\phi_i}{\sqrt{3+\sin^2\phi_i}} \leq \tan\phi_{\mathrm{DP}} \leq \frac{6\sin\phi_i}{3-\sin\phi_i} \quad (1)$$

An average value, ϕ_{DP}=44°, was adopted in the FE simulation unless specifically stated. The dilation angle was not measured in the experiment and a low value of 3° was chosen to represent its limited effect on the plastic volume change during shear failure [36]. A very small value of cohesion (c=1 Pa) was used to represent the cohesionless sand and to avoid numerical difficulties at near zero stress [27, 36].

Table 1 Material properties used in the FE model

An explicit time integration scheme was employed to perform the non-linear dynamic analysis. A convergence study concerning the time increment has been performed and a time increment of the order of 1×10^{-6} s was required to achieve a stable solution. Geometric non-linearity was taken into account. To limit numerical oscillations, the default linear and quadratic viscosity pressure in Abaqus was used [27]. The viscosity pressure is not included in the material point stress.

The whole numerical simulation consisted of three main stages of analyses in a similar fashion as in the experiment, namely the filling process, the storage process, and the discharge process. The filling process in the silo was modelled by dividing the final geometry of the solid fill into eight layers vertically. Each layer was activated sequentially starting from the bottom layer. The numerical analysis

involved achieving equilibrium for each activated layer under the load of gravity before the next layer was laid on with an initial ‘‘stress free’’ state, thereby simulating the progressive filling process [37]. To avoid numerical oscillation due to sudden loading, the load of gravity for every layer was applied incrementally in a smooth manner by using the 3rd order built-in load amplitude function in Abaqus[27]. The top surface of the granular solid was at the top level of the silo. To simulate the discharge process, a gravitational flow was considered by removing the constraints at the silo outlet instantaneously. The simulated time was 620 s in total. The period for filling was from 0 to 80 s, which was found to be sufficient for a steady filling process in the simulation. The storage period was set for 40 s. The simulated discharge process was for a duration of 500 s (from 120 s to 620 s). For a model of such size, to run a complete analysis it will take a CPU time of about 10 hours on a typical desktop PC with RAM 4 GB and processor speed 3.2 GHz. The computing time is in fact dictated by the explicit integration method which is adopted due to the involvement of high nonlinearity and softening, and in this respect the computational cost in running the ALE model is comparable to running a classical FE simulation of the same size with an explicit integration scheme.

3.2 FE model validation

To validate the FE model, the numerically predicted wall pressure and flow pattern are compared with those obtained experimentally and using analytical solutions where available. Fig.7 shows the FE predicted pressure distribution along the silo walls at the end of filling in comparison with those obtained from the experiment and classical theory. The experimental results of the filling pressure were obtained from the data averaged over a one-minute period after the end of filling. The averaged pressures are determined by the following equation:

$$\overline{p}_{wn} = \frac{1}{N}\sum_{i=1}^{N} p_{wn(i)} \tag{2}$$

where $p_{wn(i)}$ represents the normal pressure at a specified wall point at the i-th time point and $\overline{p}_{wn}$ is the averaged normal pressure at the corresponding wall point from the N time points within the period of interest.

The filling pressures were also calculated using Janssen's formula [1]. The theory for deep silos is generally based on the differential equation of the vertical equilibrium for a horizontal slice of granular solid. The solution can be written as

$$p_{wn} = \frac{\gamma R}{2\mu_w}\,[1 - e^{-h/h_0}] \tag{3}$$

where μ_w is the coefficient of wall friction, R is the radius of the silo, γ is the unit weight of the granular solid, k is the lateral pressure ratio relating the mean vertical pressure in the solid to the normal wall pressure and is assumed to be invariant with depth, h is the depth measuring from the top surface of the solid, and $h_0 = R/2\mu_w k$.

Obviously, the choice of different values of the lateral pressure ratio k will give different predictions of the wall pressure. A detailed discussion on the k values is beyond the scope of this paper. Herein a lateral pressure ratio k of 0.46 as recommended by Eurocode 1 [38] was adopted when applying the Janssen's formula. As can be seen in Fig. 6, the predicted filling pressure from the FE simulation agrees satisfactorily with the results from the silo experiment and the Janssen equation.

Fig.7 Comparison of wall pressure distributions along the silo walls at the end of filling

For the convenience of making a comparison for the discharge between the experiment and the

numerical simulation, a reference scale is required to distinguish between different stages of discharge. To this end, a discharge volume percentage is introduced to evaluate the emptying progress of the material. The volume percentage, V_{dis}, can be determined by the following equation:

$$V_{dis} = \frac{V_0 - V'}{V_0} \times 100\% \quad (4)$$

where V' is the transient volume of material left in the silo during discharge, and V_0 is the total volume of stored material prior to the discharge. The flow was observed to reach a steady state when the discharge volume percentage reached about 10% both for the silo experiments (about 4 minutes after discharge started) and the numerical simulation.

Fig.8 shows the time-averaged discharge pressure distribution along the silo walls in the early stages of discharge in the flat-bottomed silo. The experimentally measured pressures were temporally averaged over the first 4 minutes from since the start of discharge. The numerically predicted pressures were obtained by averaging over the first 60 s after discharge started (with a volume percentage of 10%), at which stage the silo was considered to have an equivalent emptying progress between the experiment and the numerical simulation. The discharge pressures on the silo walls were also calculated according to Eurocode 1 using a multiplier C=1.2 applied to the filling pressures obtained from Janssen's solution[38]. Fig.8 shows that the pressures predicted by the FE model match very well those measured in the experiment throughout the entire height of the silo. Some discrepancy between the FE and Eurocode prediction can be seen near the upper and lower boundaries. This is not surprising since Janssen's solution used in the Eurocode for the discharge state complies with the static equilibrium, whereas in the numerical simulation the dynamic equilibrium is enforced so that the varying filling level of the stored solid and the flow development are all represented.

Fig.8 Wall pressure distribution along the silo walls during discharge

As can be seen in Fig.8, both the predicted and measured pressures exhibited a maximum wall pressure of about 4 kPa which was located at the intersection of the flow channel boundary at the wall, (at about 1.0 m from the bottom of the silo). The pressure then decreased steeply to a value of about 3kPa at the bottom. This intersection on the wall may vary in time and location in correspondence with the flow development. A good understanding of such a phenomenon is important in silo design.

Fig.9 shows the time histories of wall pressure at different levels of the flat bottomed silo predicted by the FE model. Note that the reference scale as previously defined was used to correlate the wall pressure time evolution when making a comparison between the experiment and the numerical simulation. Comparing with the experimental results shown in Fig. 3, the FE model predicted similar wall pressure patterns for all levels. In general, the pressures exhibited a rise in magnitude with varying degree of fluctuations as soon as discharge started. Stronger fluctuations occurred when the material was flowing against the silo walls and directly over the pressure cells which took place above the effective transition level where the flow boundary intersected the silo walls. Below the effective transition in the lower part of the silo, the smaller fluctuations were associated with internal flow channel where there was effectively no flow against the silo walls. These characteristics of the wall pressure are in good agreement with the observation in the experiment. Similar findings have been reported in a square steel silo [39]. A detailed discussion about the flow behaviour will be given in Section 4 below.

Fig.9 Time histories of normal wall pressure at seven different levels predicted by the FE model

The flow pattern within the silo as predicted by the numerical simulation is also compared with that observed in the experiment. As described earlier, the ALE technique employed in the present FE simulation has an obvious advantage in modelling the material large deformation associated with the granular flow inside the silo. In the FE simulation, virtual tracers were used to track the corresponding material points during the analysis. The local material deformation was thus captured, from which the flow pattern can be inferred.

The spatial distributions of the tracers at four different stages of discharge are shown in Fig.10. In the upper part of the silo, the tracers exhibit a uniform (almost horizontal) profile except those at locations very close to the silo wall which tend to move downwards at a slower velocity. In the lower part of the silo, a non-uniform profile is clearly seen where the tracers towards the central axis move downwards faster than those closer to the silo walls; in fact the tracers situated at the silo bottom away from the outlet did not move since discharge started. This movement profile indicated a semi-mass flow for the flat-bottomed silo which resembles very well the observation from the silo experiment as shown in Fig.5.

Fig.11 shows the contours of the velocity vector profile in the lower part of the silo at the four stages of discharge process to further identify the flow pattern developed in the silo. The velocity vectors had a higher magnitude at and around the outlet region, as can be expected. The rather uniform distribution of velocities in much of the remaining space above (hence the contours for the upper half part is not necessary to show and those for the lower part are sufficient to identify the flow pattern developed in the silo.) indicates that the granular solid in the upper part of the silo are generally in a constant motion. The absence of velocity vectors (zero velocities) in the lower-right space, on the other hand, suggests that the granular solid in this region was essentially stationary. Such a velocity profile further confirms

a semi-mass flow inside the flat-bottomed silo.

Fig.10 Tracer profile at four discharge stages in the FE simulation

Fig.11 Contours of velocity vectors at four discharge stages

4. Further analysis of results and parametric investigation

4.1 Flow behaviour

The detailed flow behaviour in the flat-bottomed silo is further examined from the velocity field. Fig.12 shows the radial distributions of the vertical velocity component at various height levels (h=0.1m, h=0.2 m, h=0.3 m, h=0.4 m, h=0.5 m h=0.6 m h=0.8 m, h=1.0 m and h=1.4m) for different discharge stages. Fig.12(a) to (d) depicts the evolution of geometry of the flowing zone using the velocity profile. For each stage, the profile is truncated at a height above which the velocity profile becomes uniform. For the convenience of observation, the normalised vertical velocity u' is employed as follows

$$u' = -\frac{u}{u_0} \tag{5}$$

where u is the actual vertical velocity component, and u_0 is the vertical velocity component along the centreline at the level of h=0 m when a steady flow was reached. Negative values represent the downwards direction.

From Fig.12 (a), it can be seen that at the very early stage, more specifically about 10 s of discharge herein, only a small portion of solid particles near the outlet region was in motion. A narrow channel-like flowing zone formed with a width of about the outlet size and a height of 0.6 m. Along the radius of the silo, the material attained higher velocity towards the central axis. At this specific

time, the highest normalised vertical velocity at the central axis at the outlet (h=0 m) was u'=0.33, i.e., 33% of the highest velocity that would be reached in subsequent steady flow condition.

As the flow developed, see Fig.12 (b) and (c), the vertical velocity increased in most part of the silo and the flowing zone extended upwards and radially outwards from the outlet region. At the stage of V_{dis}=10%, which is shown in Fig.12(d), a steady flow was reached, after that the flowing zone size and velocity value did not change noticeably. When the steady flow was reached, a largely uniform velocity profile was established across the radius of silo at the level of h=0.7 m. Below this height, the velocity profile was not uniform and became increasingly more concentrated towards the outlet region at lower levels.

Fig.12 Radial cross-section profiles of vertical velocity at various levels at different stages. u is the actual vertical velocity component, and u_0 is the vertical velocity component along the centreline at the level of h=0 m when a steady flow was reached. Negative values represent the downwards direction.

Based on the detailed velocity field data discussed above, the flow channel boundary, which is defined as the interface between flowing and stationary material [40], can be readily identified. For this purpose, a ratio of critical velocity (RCV) is introduced as a criterion to delineate the boundary between the "flowing" particles from the "stationary" ones:

$$\mathrm{RCV} = \frac{u'}{u_0'} \tag{6}$$

where u' denotes the normalised vertical velocity of a particle at a given position, u_0' is the normalised vertical velocity of the particle at the centre position of the corresponding level, which represents the highest vertical velocity at the level.

A series of RCV values (0.1, 0.01, 0.001) were considered in the analysis for the steady flow (V_{dis}=10%) and the corresponding results are shown in Fig.13. The RCV=0.001 gave a convergent result of the flow channel boundary. Using RCV=0.001, a converging channel boundary was obtained and it intersected the wall at the height of 0.7 m, which is consistent with the experimental observation where an intersection of about 0.7~1.0 m high was observed.

To check if the criterion of RCV=0.001 may be suitable for extended applications, further verification was carried out with respect to the evolution of the flow channel boundary during different discharge stages, as shown in Fig.14. From this figure, it is clearly seen that an elliptic flowing zone, which was first reported by Kvapil [41], formed near the outlet region at early discharge stages (herein V_{dis}=0.1%). As the discharge progressed and the flow developed (V_{dis}=3% and 6% herein), the flow boundary moved upwards and radially towards the silo walls, and intersected the wall at heights of about 1.4 m and 1.0 m, respectively. This implies that the previous stagnant parts of the solid particles were increasingly activated and participated in the flow. The flowing zone extended and the boundary-wall intersection slid down until a steady flow was reached (V_{dis}=10%). The intersection then stayed at the height of 0.7m. These predictions are in good agreement with the observation of the variation of the flow boundary-wall intersection in the experiment. Similar evolution of the flow region in a flat-bottomed silo has also been reported in other experiments [42, 43]. Thus, the use of the criterion of RCV=0.001 for an explicit identification of the flow boundary is deemed to be appropriate.

Fig.13 Flow channel boundary identified using different RCVs

Fig.14 Evolution of flow channel boundary identified using RCV=0.001

4.2 Influences of varying internal friction angle

A parametric study was carried out to further investigate the flow profile with varying internal friction angles of the sand, which is the predominant parameter governing the shear strength of the cohesionless sand considered in this study. In addition to ϕ_{DP}=44º, two further internal friction angles of 34º and 54º were considered in the Drucker-Prager (DP) failure criterion in the FE simulation. The three DP internal friction angles of 34º, 44º and 54º respectively represents a real effective internal friction angle of 24º, 35º and 43º for sand.

The radial cross-sectional profiles of vertical velocity at different levels in the steady flow for three different internal friction angles are depicted in Fig. 15 in conjunction with Fig.12 (d). The three sets of results show generally similar profiles, the characteristics of which have been discussed in the previous section. The velocity distribution along the cross section became increasingly smoother at higher levels, but the height level at which it became almost uniform was markedly different among the three different internal friction cases. The case with the lowest friction angle of ϕ_{DP}=34° achieved a uniform velocity profile at the level of about 0.5 m, much faster than the 44° case at level of 0.7 m and the 54° case at level of 1.0 m, as shown in combination in Fig. 16. Due to the flat-bottomed geometry of the silo, a stagnant zone, which is depicted by the flow channel boundary in Fig. 16, always formed at the silo bottom away from the outlet but with different sizes for the three internal friction angles. The results suggest that a granular material with a lower internal friction angle, and hence lower shear strength, tend to flow more easily than one with a higher internal friction angle or higher shear strength. It is expected that the material with a higher shear strength will reach the angle of repose and therefore cascade down the higher level [42]. A similar observation has also been reported in an experimental investigation of cylindrical hopper [44]. The trend of the numerical results indicates that

such a condition can be clearly reproduced from the present FE model.

Fig. 15 Radial cross-section profiles of vertical velocity for the steady flow using different internal friction angles

Fig. 16 Flow channel boundaries at steady flow predicted using different internal friction angles

The flow channel boundary can also be characterised by the high local shear stress within the material. Fig. 17 shows the profiles of shear stress within the material at steady flow for three different internal friction angles. It can be seen that for all the three cases there is a kink or jump of shear stress at relatively low position levels, but as the height increases the kink becomes less pronounced and finally a rather uniform shear stress profile appears. The location of the kink in the shear stress profile corresponds closely to the boundary between the flowing and stagnant zones at each level as shown in Fig. 16. The position where the kink occurs indicates that the material experiences a high shear stress resulting potentially in a shear failure. This can be confirmed by the contours of the equivalent plastic strain as shown in Fig. 18. It is worth noting that the size of the shear zone in the present simulation may depend, to a certain extent, on the mesh size since the constitutive model adopted does not involve a characteristic length relating to the micro-structure of granular solid. For the material with a higher shear strength (herein with ϕ_{DP}=54°), a failure plane appears to occur within the high velocity flow, which is located in the central region of the flow. Consequently, the material of ϕ_{DP}=54° has a flow channel boundary with a steeper slope against the horizon than those of relatively low internal friction angles, i.e., ϕ_{DP}=44° and 34°. A larger stagnant zone would be expected to form when the stored granular material of high shear strength is withdrawn from the flat-bottomed silos.

A scenario with smooth silo walls, where the coefficient of wall friction is set to be a very small value of 0.01, has also been considered in the FE simulation. Contours of the solid deformation are shown in Fig. 19 as a comparison with the reference case where the wall friction coefficient, μ_{wd}, is set to the experimentally measured value of 0.5. With negligible wall friction, the material moves with a more uniform velocity and deformation across the radius of the silo. The wall shear zone, which characterises a frictional solid-wall interaction in the reference case, has disappeared for all the three solid internal friction angles. Instead, the flowing zone expands radially with relatively low intersection of the flow channel boundary at the wall.

Fig. 17 Radial cross-section profiles of shear stress for steady flow using different internal friction angles

Fig. 18 Contours of equivalent plastic strain for steady flow using three different internal friction angles with the reference case of wall friction (μ_{wd}=0.5)

Fig. 19 Contours of equivalent plastic strain for steady flow using three different internal friction angles with smooth walls (μ_{dw}=0.01)

5. Conclusions

A FE model using the ALE technique is developed for the detailed analysis of the granular flow in flat-bottomed silos in this paper. By defining appropriate ALE boundaries and a suitable numerical integration strategy, the model can simulate the entire filling and discharge process, thus allowing for a numerical investigation of the characteristics of the flow behaviour inside the silo and the dynamic pressure on the silo walls.

The FE model is validated against an experimental study involving a large-size laboratory model silo, as well as suitable theoretical solutions. The spatial distributions of the filling and discharge pressures along the silo walls predicted by the FE model agree well with Janssen's solution and the experimental results. More specifically, an apparent change of discharge wall pressure at a certain height (about 1.0 m in the case under consideration) was obtained by both the FE model and the silo experiment, and this is consistent with the general understanding in a semi-mass flow scenario. From the time histories of wall pressure, the FE model predicts a notable increase (about 25%)in the amplitude of the discharge pressure as compared to the filling pressure in most part of the silo walls, and this is also consistent with the experimental measurement. With the use of the tracer technique in the ALE approach, a semi-mass flow pattern can be clearly delineated from the FE simulation results.

To gain further understanding of the flow behaviour in flat-bottomed silos, a criterion for identifying the flow channel boundary has been proposed based on the ratio of vertical velocity across the radius of the silo at different levels. Using the criterion, a gradually growing flow zone which initiates near the outlet can be identified during the silo discharge simulation. At the fully developed flow state, the flow zone can be described as a converging zone with the velocity profile concentrated towards the outlet at the lower part of the silo, which reflects a special characteristic associated with the flat-bottomed geometry of the silo.

Furthermore, the influence of shear strength of the stored granular material on the flow behaviour has been investigated through varying the key parameter of the internal friction angle for cohesionless sand. The results demonstrate that a granular material with a low shear strength flows more easily than a material with a higher shear strength. A larger stagnant zone can be expected to form when a material with a higher shear strength is withdrawn from a flat-bottomed silo. Smoothing walls appears to be an

beneficial operation for improving flow behaviour of material out of the silos. The characterisation of the flow behaviour and the dynamic wall pressures can be very useful in silo design.

Due to the limitation of the constitutive mode used in the present FE model, the details of the complex granular flow behaviour may not be captured realistically at this stage. To pursue such flow behaviour, an advanced constitutive model must be employed, in which the pressure effect, the density effect, the deformation rate effect and grain size effect should also be considered. The development of such a model will allow a comprehensive investigation of the micro-structure of the granular flow and this is to be considered in the future work.

Acknowledgements

The author Y.W. would like to acknowledge the support from 'the Fundamental Research Funds for the Central Universities' (Grant No. DUT13RC(3)66) and the National Basic Research Program of China (973 Program) (Grant No. 2014CB047100).

References

[1] H.A. Janseen, Versuche uber getreidedruck in silozellen. Zeitschrift des Vereines Deuischer Ingenieure 39 (35) (1895) 1045-1049.

[2] A.W. Jenike, J.R. Johanson, J.W. Carson, Bin loads-part 3: mass flow bins, J. Eng. Ind. Trans. ASME 95 (1) (1973) 6-12.

[3] U. Tuzun, R.M. Nedderman, A kinematic model for the flow of granular materials. Powder Technology 22 (1979) 243-253.

[4] J.Y. Ooi, J.M. Rotter, Measured pressures in full scale silos: A new understanding. Proc. Bulk 2000: Bulk Mat. Handling-Towards the Year 2000. Institute of Mechanical Engineers, London; 1991. p.

195-200.

[5] J. Munch-Andersen, V. Askegaard, A. Brink, Silo model tests with sand. Bulletin No. 91, Danish Building Research Institute; 1992.

[6] Z. Zhong, J.Y. Ooi, J.M. Rotter, The sensitivity of silo flow and wall stresses to filling method. Engineering Structures 23 (2001) 756-767.

[7] S. Ding, J.M. Rotter, J.Y. Ooi, G. Enstad, D. Xu, Normal pressures and frictional tractions on shallow conical hopper walls after concentric filling: predictions and experiments, Chem. Eng. Sci. 89 (2013) 264–272.

[8] F. Ayugy, Some unresolved problems in the design of steel cylindrical silos. Crc. Press-Talyor Francis Group, Boca Raton; 2008.

[9] J.Y. Ooi, J.M. Rotter, Wall pressures in squat steel silos from simple finite element analysis. Computer & Structures 27(4) (1990) 361-374.

[10] J.M. Rotter, C.J. Brown, E.H. Lahlouh, Patterns of wall pressure on filling a square planform steel silo. Engineering Structures 24 (2002) 135-150.

[11] J.M. Rotter, Guide for the Economic Design of Circular Metal Silos, Spon, London, 2001.

[12] P.M. Blair-Fish, P.L. Bransby, Flow patterns and wall stresses in a mass-flow bunker. Journal of Engineering for Industry 2 (1973) 17-26.

[13] S. Masson, J. Martinez, Effect of particle mechanical properties on silo flow and stresses from distinct element simulation. Powder Technology 109 (2000) 164-178.

[14] C.S. Chou, J. Smid, R.Y. Chen, Flow patterns and stresses on the wall in a two-dimensional flat-bottomed bin. Journal of Chinese Institute of Engineer 26(4) (2003) 397-408.

[15] J. Härtl, J.Y. Ooi, J.M. Rotter, M. Wojcik, S. Ding, G.G. Enstad, The influence of cone-in-cone

insert on flow pattern and wall pressure in a full scale silo. Chemical Engineering Research and Design 86 (2008) 370-378.

[16] A. Ramírez, J. Nielsen, F. Ayuga, On the use of plate-type normal pressure cells in silos Part 1: calibration and evaluation, Comput. Electron. Agric. 71 (2010): 71-76.

[17] W.R. Ketterhagen, J.S. Curtis, C.R. Wassgren, B.C. Hancock, Predicting the flow mode from hoppers using the discrete element method. Powder Technology 195 (2009) 1-10.

[18] A. Ramírez. J. Nielsen, F. Ayuga, On the use of plate-type normal pressure cells in silos. Part 2: Validation for pressure measurements. Comput. Electron. Agric. 71 (2010) 64–70.

[19] Y. Yang, J.Y. Ooi, J.M. Rotter, Y. Wang, Numerical analysis of silo behavior using non-coaxial models. Chemical Engineering Science 66 (2011) 1715-1727.

[20] R. Balevicius, I. Sielamowicz, Z. Mroz, R. Kacianauskas, Effect of rolling friction on wall pressure, discharge velocity, outflow of granular material from a flat-bottomed bin. Particuology 10 (2012) 672-682.

[21] M. Wójcik, J. Tejchman, Modeling of shear localization during confined granular flow in silos within non-local hypoplasticity. Powder Technology 192 (2009) 298-310.

[22] Y. Xu, K.D. Kafui, C. Thornton, G. Lian, Effects of material properties on granular flow in silo using DEM simulation. Particulate Science and Technology 20 (2002) 109-124.

[23] P.W. Cleary, M.L. Sawley, DEM modelling of industrial granular flow: 3D case studies and the effect of particle shape on hopper discharge. Applied Mathematical Modelling 26 (2002) 89-111.

[24] M.A. Martinez, I. Alfaro, M. Doblare, Simulation of axisymmetric discharging in metallic silos: Analysis of the induced pressure distribution and comparison with different standards. Engineering Structures 24 (2002) 1561-1574.

[25] P. Vidal, M. Guaita, F. Ayuga, Analysis of dynamic discharge pressures in cylindrical slender silos with a flat bottom or with a hopper: comparison with Eurocode 1. Biosystems Engineering 91(3) (2005) 335-348.

[26] J. Donea, A. Huerta, Finite element method for flow problems, Wiley Press, 2003.

[27] SIMULIA. Abaqus analysis: User's Manual. Dassault Systèmes, 2008.

[28] Y. Wang, Y. Lu, J.Y. Ooi, Numerical modelling of dynamic pressure and flow in hopper discharge using the Arbitrary Lagrangian-Eulerian formulation. Eng. Struct. 56 (2013) 1308-1320.

[29] Y. Wang, Y. Lu, J.Y. Ooi, Finite element modelling of wall pressure in a cylindrical silo with conical hopper using an Arbitrary Lagrangian-Eulerian formulation. Powder Technology 257 (2014) 181-190.

[30] J.M. Rotter, J.Y. Ooi, Z. Zhong, Danish silo experiment: Unsymmetrical wall pressure measurements, Internal Report, School of Engineering, University of Edinburgh, Edinburgh, 2004.

[31] V. Askegaard, J. Munch-Andersen, Results from tests with normal and shear stress cells in a medium-scale model silo, Powder Technology 44 (1985) 151-157.

[32] J.F. Chen, J.M. Rotter, J.Y. Ooi, Z. Zhong, Flow pattern measurement in a full scale silo containing iron ore. Chemical Engineering Science 60 (2005) 3029-3041.

[33] D.C. Drucker, W. Prager, Soil mechanics and plastic analysis on limit design. Quarterly Applied Mathematics 10(2) (1952) 157-165.

[34] S. Ding, Investigations of flow and pressure in silos during filling and discharging in presence of inserts, Ph.D. thesis, The University of Edinburgh, UK, 2004.

[35] M. Wojcik, J. Härtl, J.Y. Ooi, J.M. Rotter, S. Ding, G.G. Enstad, Experimental investigation of the flow pattern and wall pressure distribution in a silo with a double-cone insert, Particle & Particle

Systems Characterization 24(4-5) (2007) 296-303.

[36] J. Ai, J.F. Chen, J.Y. Ooi, Finite element simulation of the pressure dip in sandpiles, International Journal of Solids and Structures 50 (2013) 981-995.

[37] J. Ai, J.F. Chen, J.M. Rotter, J.Y. Ooi, Numerical and experimental studies of the base pressures beneath stockpiles, Granul. Matter 13 (2011) 133-141.

[38] EN 1991-4. Eurocode 1: Actions on Structures. Silos and Tanks. Brussel: CEN 2006.

[39] C.J. Brown, E.H. Lahlouha, J.M. Rotter, Experiments on a planform steel silo. Chemical Engineering Science 5 (2000) 4399-4413.

[40] G.R. Watson, J.M. Rotter, A finite element kinematic analysis of planar granular solids flow. Chemical Engineering Science 51(16) 1996 3967-3978.

[41] R. Kvapil, Theorie der Schuttgutbewegung, Berlin, VEB-VerlagTechnik, 1959.

[42] G.R. Watson, Flow patterns in flat bottomed silos, Ph.D thesis, The University of Edinburgh, UK, 1993.

[43] I. Sielamowicz, M. Czech, T.A. Kowalewski, Empirical description of granular flow inside a model silo with vertical walls. Biosystems Engineering 108 (2011) 334-344.

[44] A. Gupta, S. Nag, V. Tathavadkar, Predicting flow mode in cylindrical hopper, International Journal of Mineral Processing 110-111 (2012) 135-139.

Table 1 Material properties used in the FE model

Physical parameters	Value
Average unit weight γ (kN/m^3)	14.2
Measured internal friction angle (ϕ_i)	35
DP internal friction angle ϕ_{DP}(º)	44
DP dilation angle ψ (º)	3
DP cohesion c (Pa)	1
Young's Modulus (MPa)	2.0
Coefficient of wall friction (μ_w)	0.6

Fig.20 The experimental setup

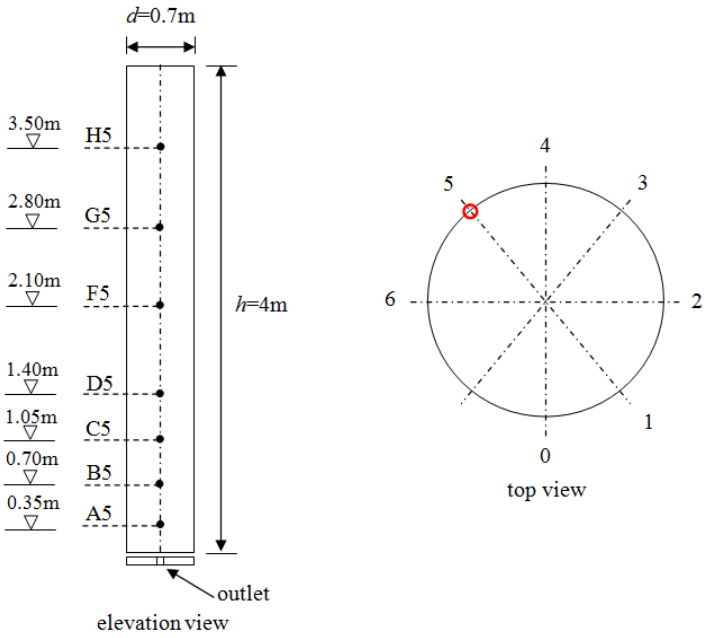

Fig.21 Schematic diagram of layout of pressure cell on the silo walls

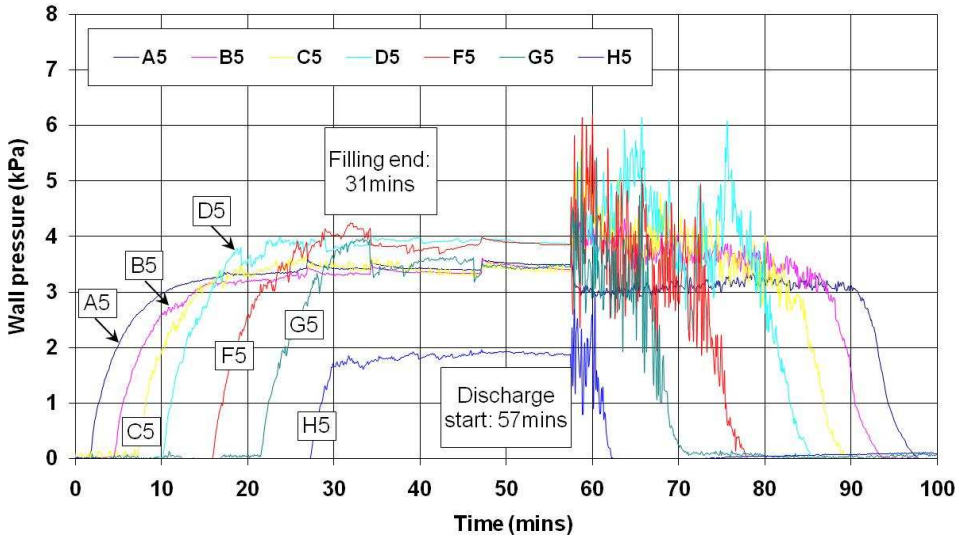

Fig.22 Time history of wall normal pressure measured by seven pressure cells at different levels (redrawn after Rotter et al. [26])

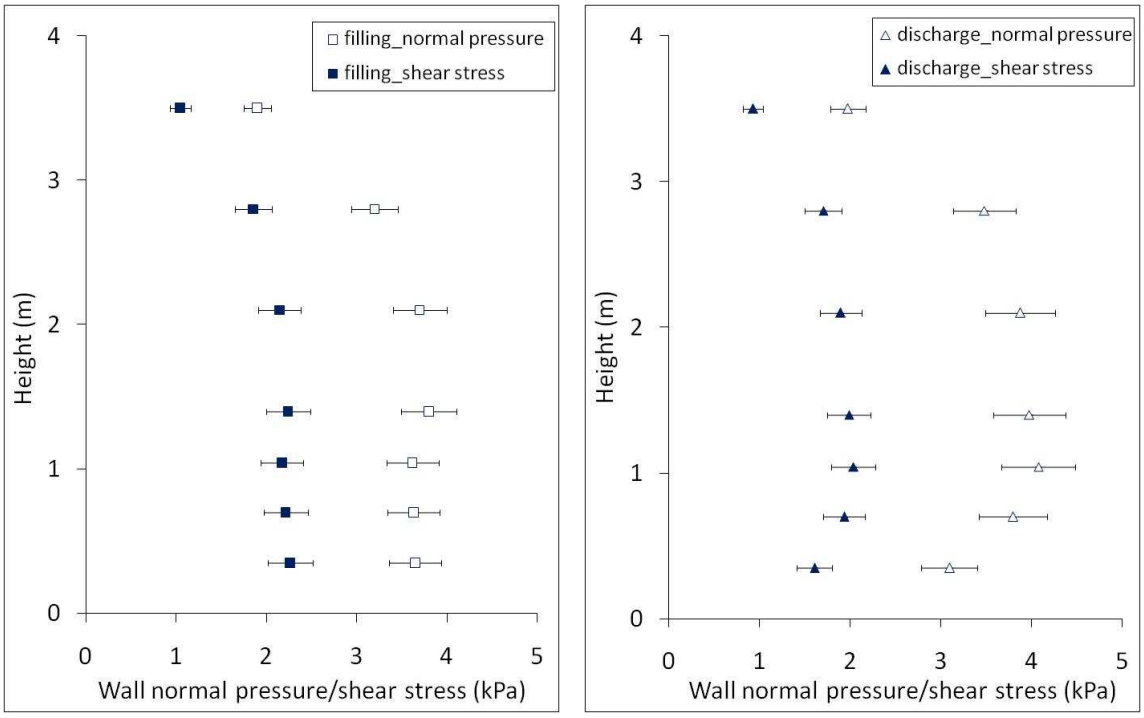

Fig. 23 Stress distributions measured to determine the coefficient of wall friction at different levels during filling and discharge in the silo tests (Redrawn after Rotter et al. [30])

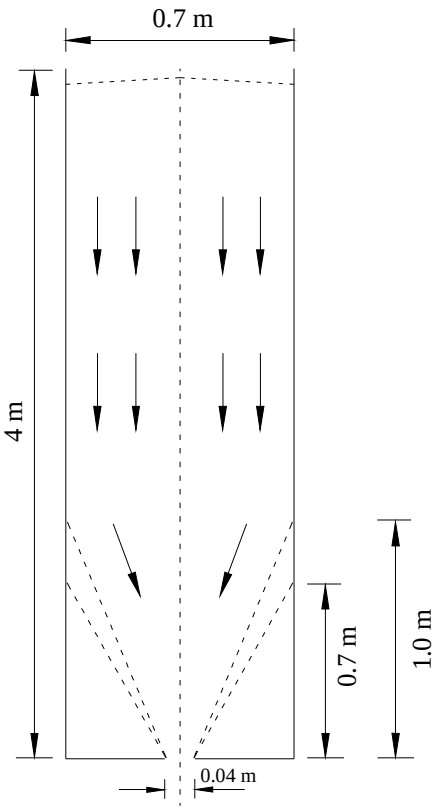

Fig.5 Flow channel boundary during the flat-bottomed silo discharge (Redrawn after Rotter et al. [26])

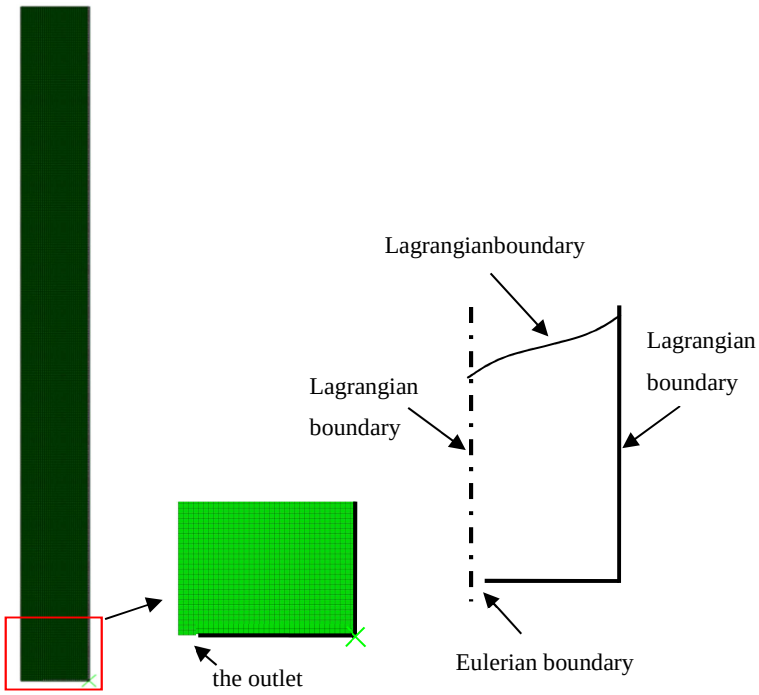

Fig. 6 FE mesh configuration and ALE boundaries

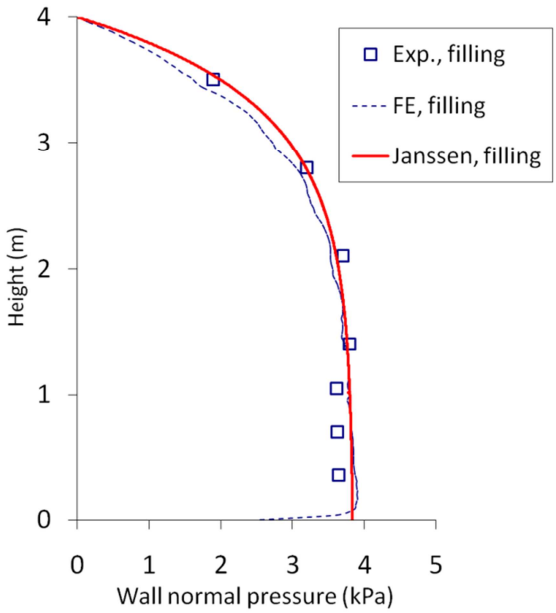

Fig. 7 Comparison of wall pressure distributions along the silo walls at the end of filling

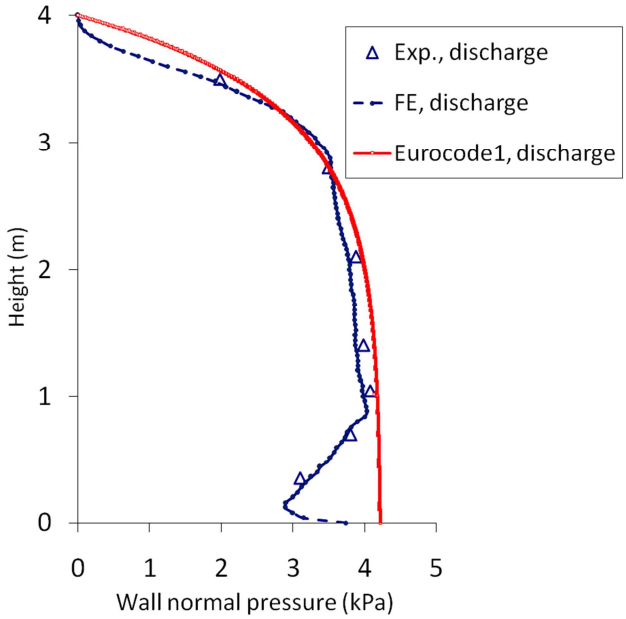

Fig. 8 Wall pressure distribution along the silo walls during discharge

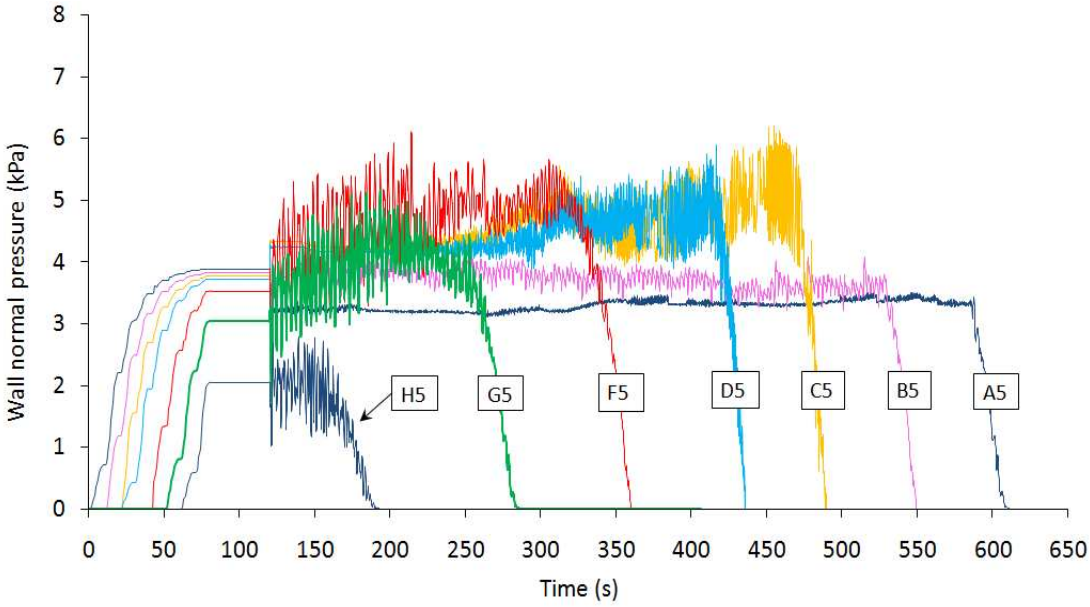

Fig. 9 Time histories of normal wall pressure at seven different levels predicted by the FE model

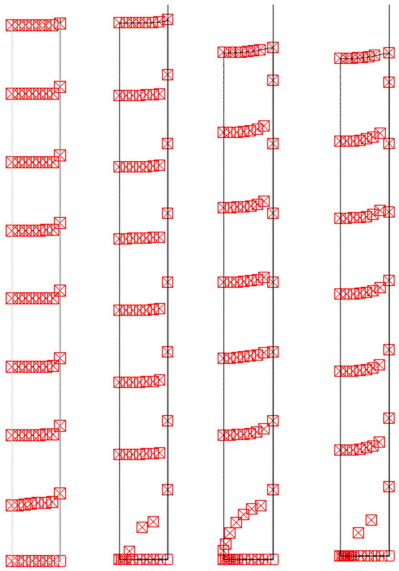

t_{dis}=10s, V_{dis}=0.1%;t_{dis}=1min, V_{dis}=3%;t_{dis}=2min, V_{dis}=6%; t_{dis}=4min, V_{dis}=10%

Fig. 10 Tracer profile at four discharge stages in the FE simulation

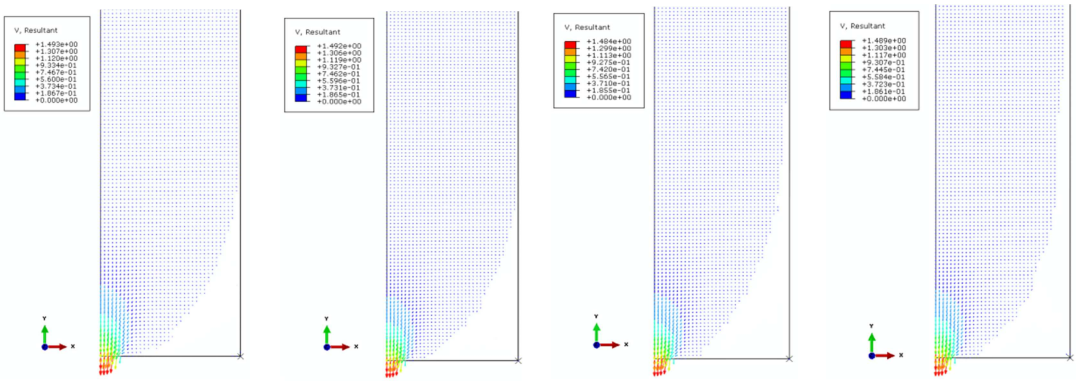

t_{dis}=10s, V_{dis}=0.1%; t_{dis}=1min, V_{dis}=3%;t_{dis}=2min, V_{dis}=6%;t_{dis}=4min, V_{dis}=10%

Fig. 11 Contours of velocity vectors at four discharge stages

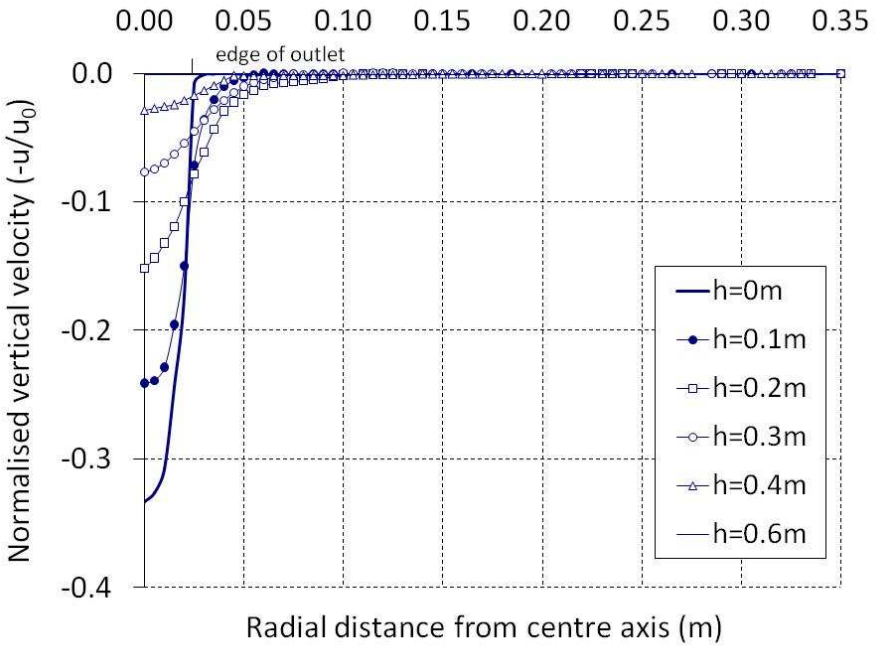

(a) at the stage of t_{dis}=10 s, V_{dis}=0.1%

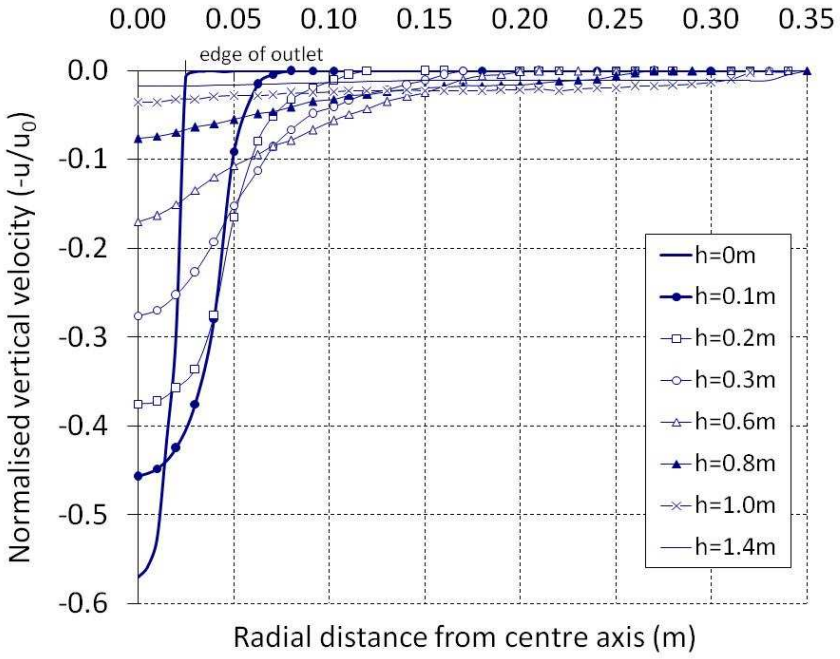

(b) at the stage of t_{dis}=1 min, V_{dis}=3%

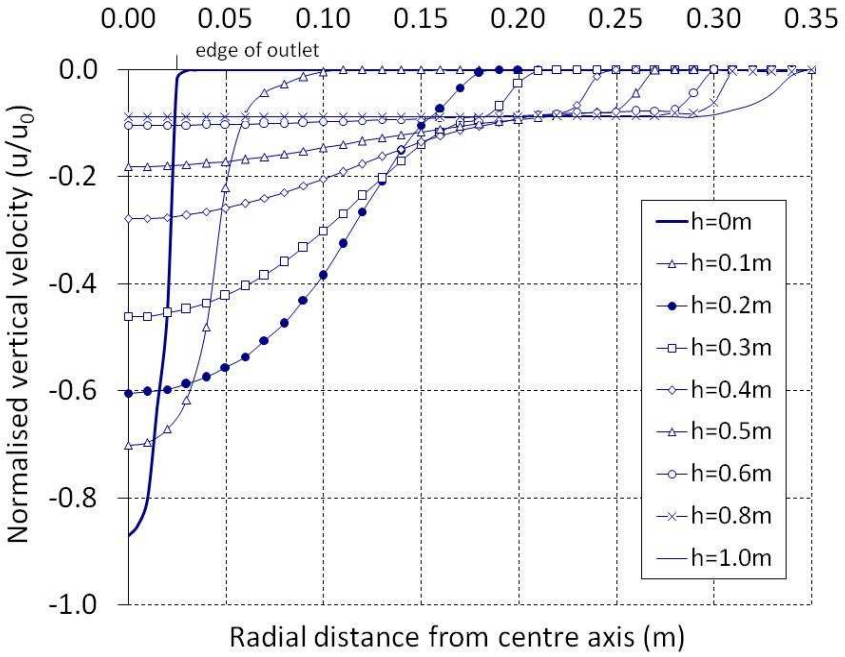

(c) at the stage of t_{dis}=2 min, V_{dis}=6%

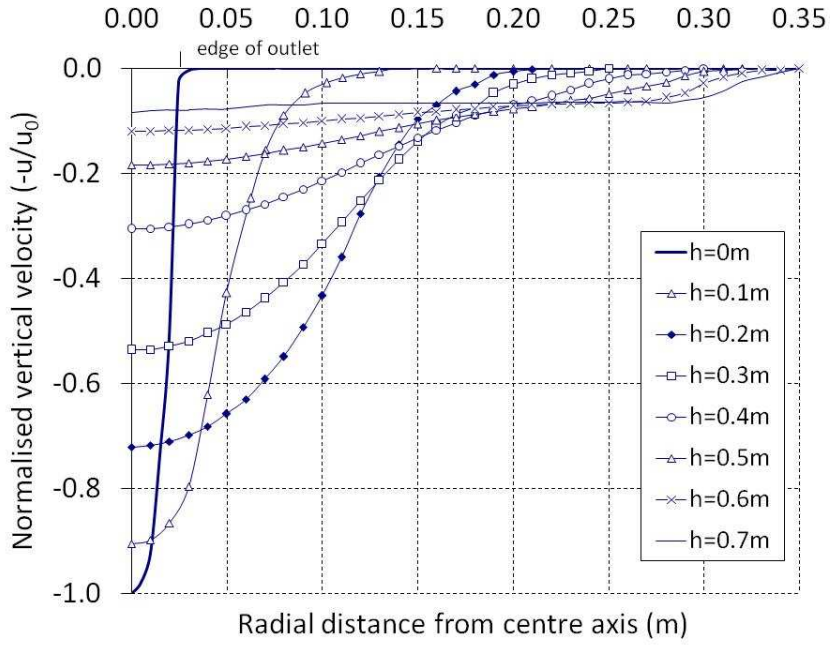

(d) at the stage of t_{dis}=4 min, V_{dis}=10%, considered as steady state flow

Fig. 12 Radial cross-section profiles of vertical velocity at various levels at different stages. u is the actual vertical velocity component, and u0 is the vertical velocity component along the centreline at the level of h= 0 m when a steady flow was reached. Negative values represent the downwards direction.

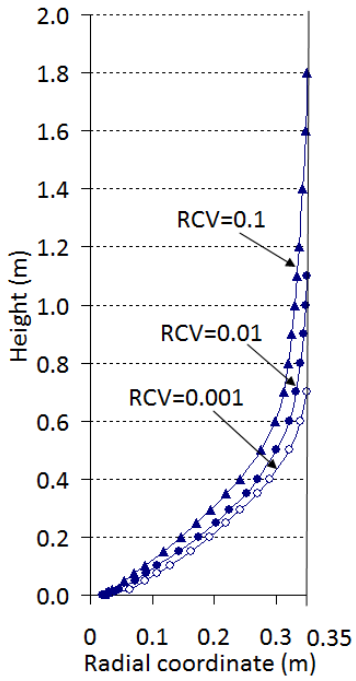

Fig. 13 Flow channel boundary identified using different RCVs

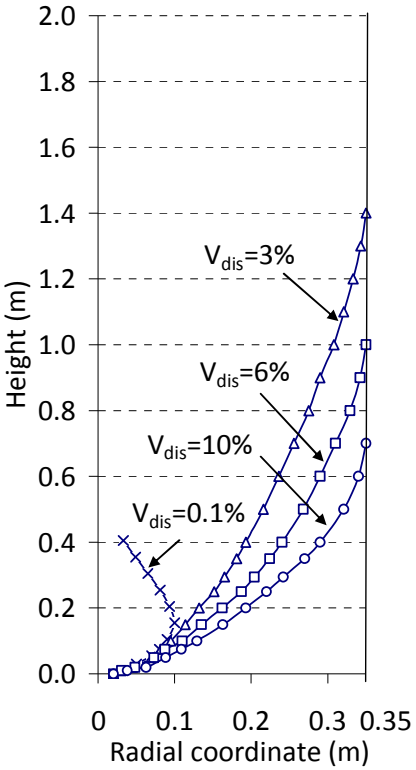

Fig. 14 Evolution of flow channel boundary identified using RCV=0.001

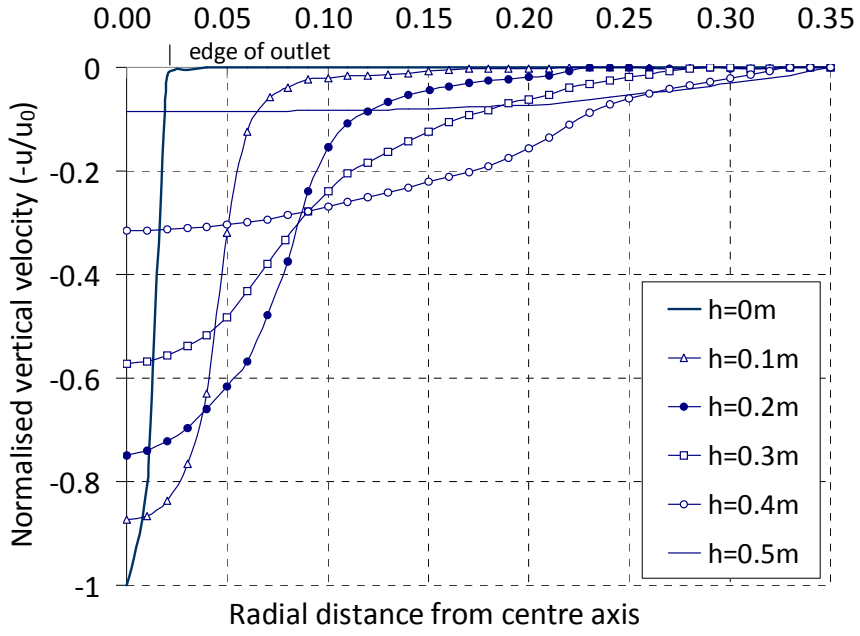

(a) ϕ_{DP}=34°

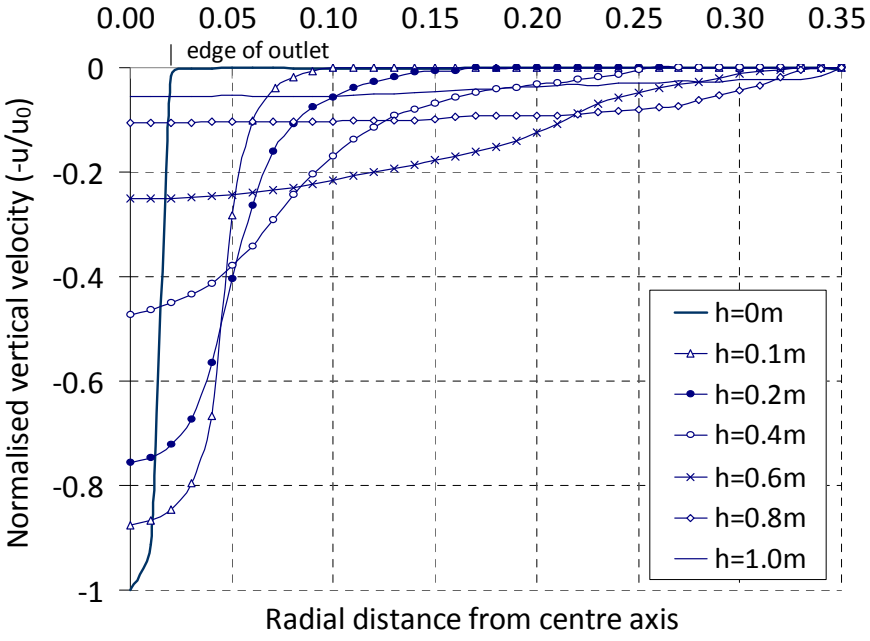

(b) ϕ_{DP}=54°

Fig. 15 Radial cross-section profiles of vertical velocity for the steady flow using different internal friction angles

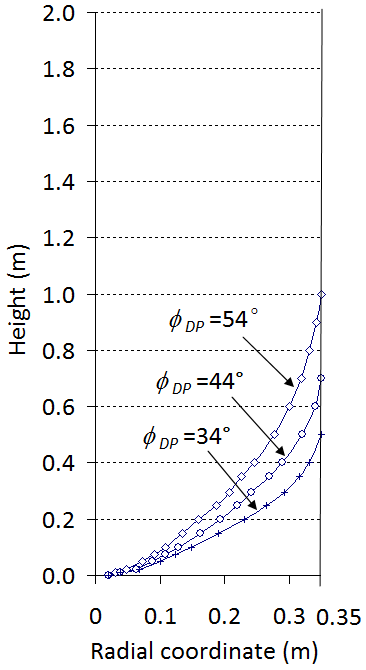

Fig. 16 Flow channel boundaries at steady flow predicted using different internal friction angles

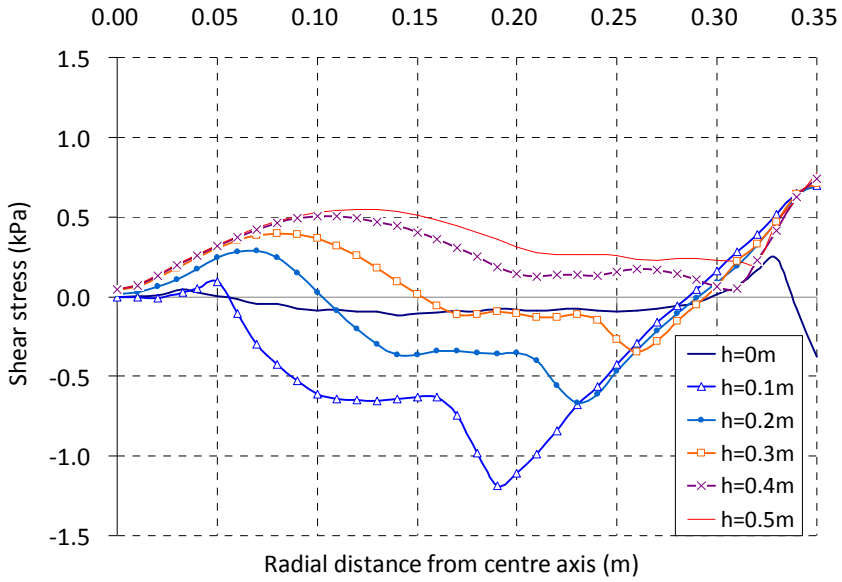

(a) ϕ_{DP}=34°

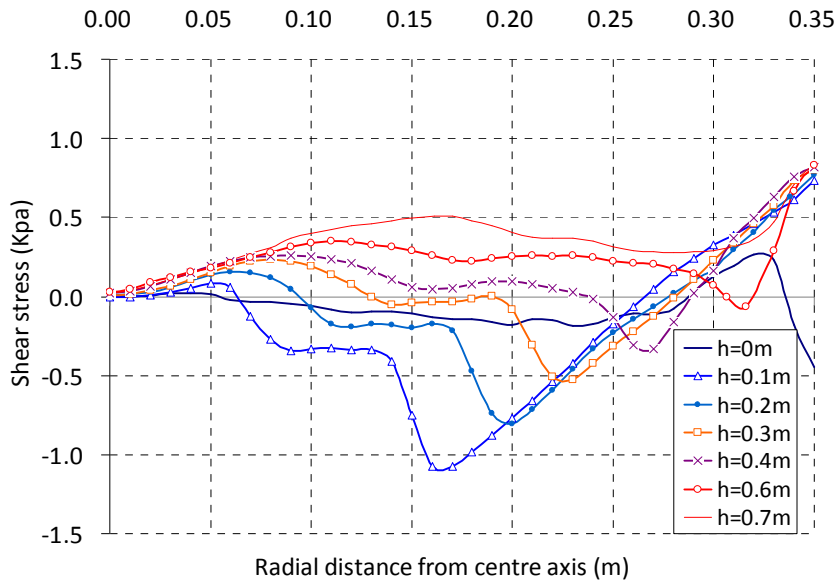

(b) ϕ_{DP}=44°

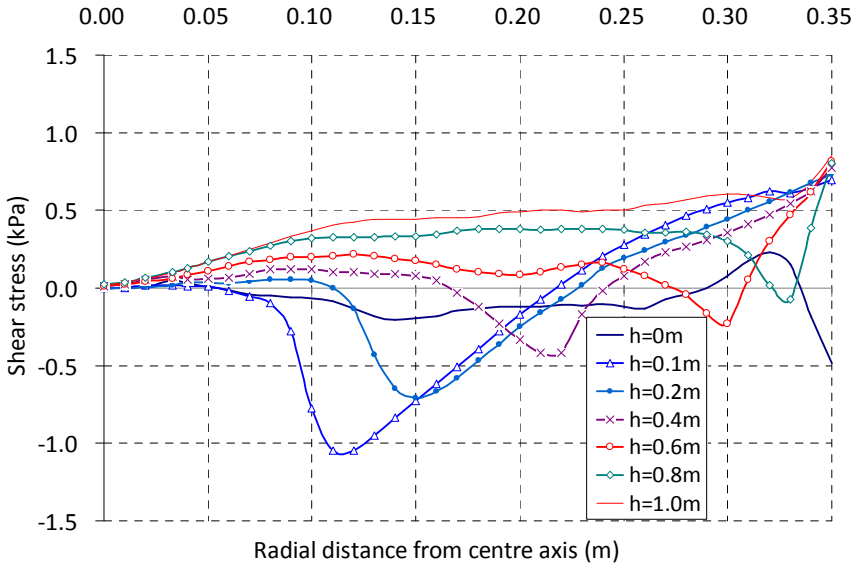

(c) ϕ_{DP}=54°

Fig. 17 Radial cross-section profiles of shear stress for steady flow using different internal friction angles

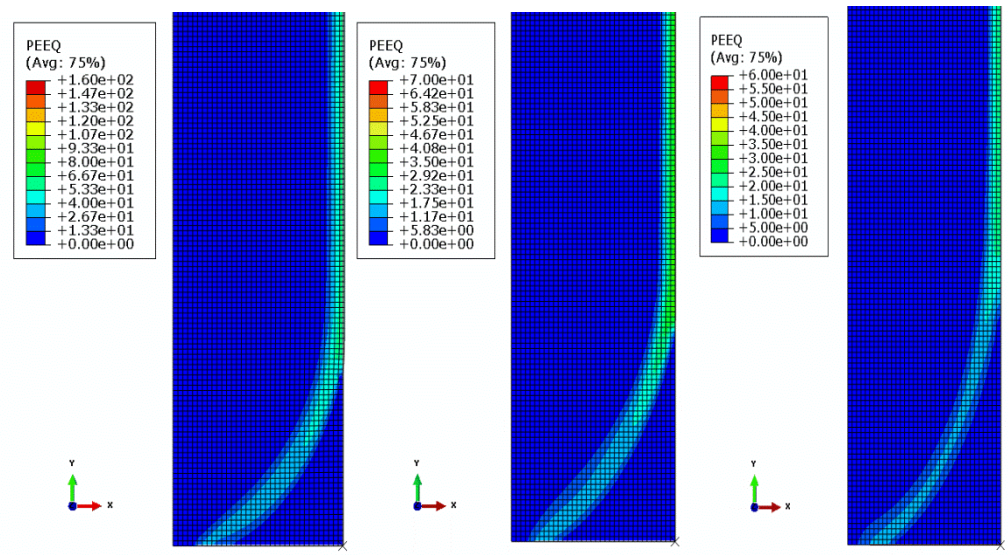

(a) ϕ_{DP}=34° (b) ϕ_{DP}=44° (c) ϕ_{DP}=54°

Fig. 18 Contours of equivalent plastic strain for steady flow using three different internal friction angles

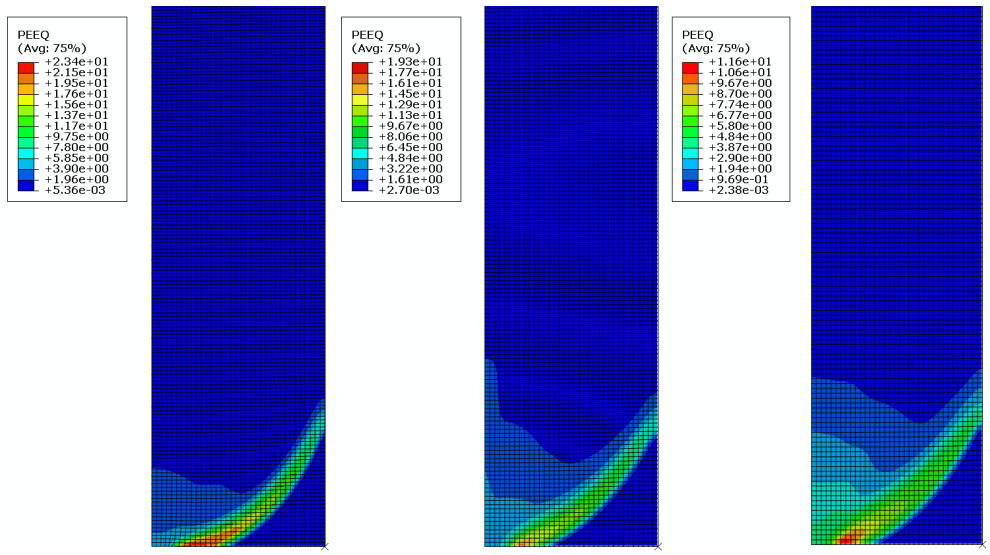

(a) ϕ_{DP}=34° (b) ϕ_{DP}=44° (c) ϕ_{DP}=54°

Fig. 19 Contours of equivalent plastic strain for steady flow using three different internal friction angles with smooth walls (μ_{wd}=0.01)